Giant-block twist grain boundary smectic phases

J. Fernsler[†], L. Hough[†], R.-F. Shao[†], J. E. Maclennan[†], L. Navailles[‡§], M. Brunet[§], N. V. Madhusudana[¶], O. Mondain-Monval[‡‖], C. Boyer[‖], J. Zasadzinski[‖], J. A. Rego[††], D. M. Walba[††], and N. A. Clark[†‡‡]

[†]Department of Physics and Liquid Crystal Materials Research Center, University of Colorado, Boulder, CO 80309-0390; [††]Department of Chemistry and Biochemistry and Liquid Crystal Materials Research Center, University of Colorado, Boulder, CO 80309-0215; [‖]Department of Chemical Engineering, University of California, Santa Barbara, CA 93106; [‡]Centre de Recherche Paul Pascal, Centre National de la Recherche Scientifique, Avenue Albert Schweitzer, 33600 Pessac, France; [¶]Raman Research Institute, Bangalore 560080, India; and [§]Groupement de Droit Comparé, Unités Mixtes de Recherche 5581, Université Montpellier II, F 34095 Montpellier Cedex 05, France

Edited by Tom C. Lubensky, University of Pennsylvania, Philadelphia, PA, and approved August 15, 2005 (received for review March 9, 2005)

Study of a diverse set of chiral smectic materials, each of which has twist grain boundary (TGB) phases over a broad temperature range and exhibits grid patterns in the Grandjean textures of the TGB helix, shows that these features arise from a common structure: ''giant'' smectic blocks of planar layers of thickness $l_b > 200$ nm terminated by GBs that are sharp, mediating large angular jumps in layer orientation between blocks ($60° < \Delta < 90°$), and lubricating the thermal contraction of the smectic layers within the blocks. This phenomenology is well described by basic theoretical models applicable in the limit that the ratio of molecular tilt penetration length-to-layer coherence length is large, and featuring GBs in which smectic ordering is weak, approaching thin, melted (nematic-like) walls. In this limit the energy cost of change of the block size is small, leading to a wide variation of block dimension, depending on preparation conditions. The models also account for the temperature dependence of the TGB helix pitch.

liquid crystal | chirality | screw dislocation | helix

The nearly simultaneous prediction of the twist grain boundary (TGB) phase, the liquid crystal (LC) analog of the Abrikosov type II superconductor (1), and its discovery in the nP1M7 series of chiral smectics (2) has led to a class of soft-matter phases exhibiting particularly striking manifestations of chirality. Although fluid-layered smectics in general tend to expel twist of the layer normal, the TGB phases adopt a state of layer twist, driven by molecular chirality in a way analogous to the accommodation of magnetic field by the formation of flux vortices in a type II superconductor. In the LC case twist is enabled by formation of GBs, which behave as arrays of screw dislocations, mediating change in layer orientation between blocks of planar smectic layers, and acting as the "flux tubes" in deGennes' smectic/superconductor analogy (3).

The early TGBs (2, 4, 5) exhibited a set of common characteristics, including narrow TGB phase temperature (T) ranges, $T_R \approx 1°C$, small angular jumps in layer orientation at the GBs (5), and Grandjean-like textures of the director rotation (TGB) helix (2). However, beginning with the 1993 report of the nitrotolane system having homologs with TGB phase ranges of up to 100°C (6), a distinct class of TGB materials has emerged (6–11) characterized by: (*i*) large T_R values ($10°C < T_R < 100°C$); (*ii*) modulated and/or undulated Grandjean textures, first described in the "UTGBC" phase of the Bangalore S1014/CE8 mixture (7) and observed in other mixtures (10, 11), as well as in neat materials (6, 8, 9)[§§]; (*iii*) evidence for large angular jumps between blocks, 90° in the case of the UTGBC square lattice (7) and 60° inferred from nitrotolane x-ray data showing 6-fold symmetric block orientation (9); and (*iv*) electric field-induced unwinding of the TGB helix (6, 12). Here, we report detailed structural studies using freeze-fracture electron microscopy (FFEM), x-ray diffraction (XRD), and depolarized transmission light microscopy of three members of this class, the 36% S1014/64% CE8 Bangalore mixture (7) and the neat Boulder nitrotolanes W371 (6) and W376 (6). Despite their distinct chemical nature, these materials, which we refer to as "giant-block" TGBs (GBTGBs), exhibit quite similar structural features. We show that the GBTGB structure occurs at the limit of TGB behavior characterized by a ratio $\kappa \equiv \lambda/\xi$ of twist penetration length, λ, to smectic layer correlation length ξ (Fig. 1*a*) that is very large, approaching $\kappa \approx 100$, with $1/\lambda \approx k_o, = 2\pi/p$, where p is the preferred pitch of the twist of the director **n,** the mean local molecular long axis orientation, without smectic layering.

Materials and Methods

FFEM was carried out by quenching the LC, sandwiched between 2×2-mm Cu planchettes, from various temperatures in the TGB range to 77 K by rapid immersion in liquid propane and fracturing it cold in a vacuum. Transmission electron microscopy of Pt-C fracture face replicas revealed topographies having the global structure of layer surfaces and layer steps familiar from the study of fluid thermotropic and lyotropic smectics (13, 14). FFEM thus provided a direct measure of the layering block structure of TGB phases, enabling direct visualization, with ≈2-nm resolution, of the mediation of layer twist by screw dislocations, the latter identifiable as terminations of layer steps (4). XRD studies of the structure factor $I(q_x, q_z)$ of W371 and W376, where q is the scattering vector (see Fig. 3), were also carried out on 20- to 30-μm-thick Grandjean-oriented samples (TGB helix axis normal to the surfaces) contained between kapton films (W371) or ≈100-μm-thick glass plates (W376).

W371, W376, and a S1014/CE8 mixture were studied. S1014 is 2-cyano-4-heptyl-phenyl-4′-pentyl-4-biphenyl carboxylate (7), and CE8 is 2′-methyl-butyl-phenyl-4′-*n*-octyl piphenyl-4-carboxylate (7). The phase sequence of the 36% S1014/64% CE8 mixture used is isotropic (I) to chiral nematic (CN) at $T = 122°C$, CN to GBTGB smectic A (GBTGBA) at $T = 77°C$, and GBTGBA to GBTGB smectic C (GBTGBC) at $T = 63°C$. W371 is 4-[4-(1-hexyloxycarbonyl-ethylamino)-3-nitro-phenylethynyl]-benzoic acid 4-(9-*cis*-12-*cis*-octadecadienyl)-oxy-phenyl ester (compound 9 in ref. 6). The phase sequence of W371 is I to CN at $T = 73°C$, CN to GBTGBA at $T = 60°C$, and GBTGBA to GBTGBC at $T = 47°C$. W376 is 4-[4-(1-hexyloxycarbonyl-ethylamino)-3-nitro-phenylethynyl]-benzoic acid 4-dodecyloxy-phenyl ester (compound 8 in ref. 6). The phase sequence of W376 is *I* to CN at $T = 98°C$, CN to GBTGBC at $T = 62°C$, and GBTGBC to crystal at $T = 48°C$. Helix pitches were measured from Grandjean line spacing in wedge cells with the helix axis normal to the plates.

Results

Fig. 2 shows examples of FFEM images of the GBTGB layering in S1014/CE8 and W376. The fracture faces exhibit domains of well ordered TGB helix (Fig. 2 *a*, *b*, and *d*), areas where the helix is

This paper was submitted directly (Track II) to the PNAS office.

Abbreviations: LC, liquid crystal; SmA, smectic A; SmC, smectic C; GB, grain boundary; TGB, twist GB; MGB, melted GB; GBTGB, giant-block TGB; GBTGBA, GBTGB smectic A; GBTGBC, GBTGB smectic C; FFEM, freeze-fracture electron microscopy; XRD, x-ray diffraction; CN, chiral nematic.

[‡‡]To whom correspondence should be addressed. E-mail: noel.clark@colorado.edu.

[§§]Clark, N. A. & Shao, R. F., University of Pennsylvania TGB Symposium, April 22–24, 1998, Philadelphia.

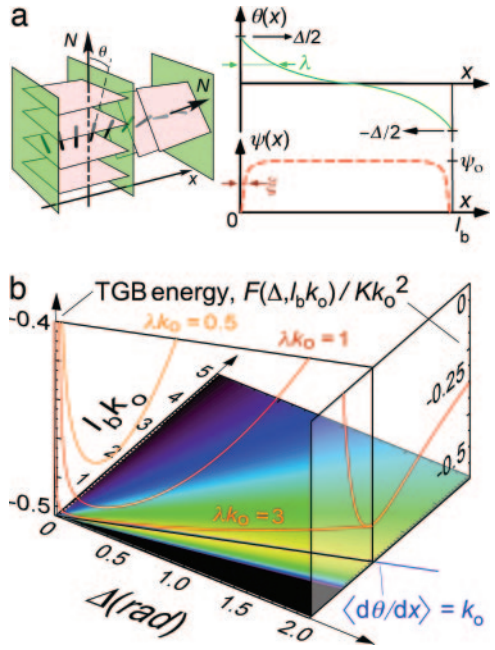

Fig. 1. GBTGBA schematic structure and model energy. (*a*) GBTGBA structure in the limit that $\lambda > \xi$ and plots showing the spatial variation of the smectic order parameter $\psi(x)$ and the director tilt $\theta(x)$ for one smectic block. The smectic blocks, of thickness l_b, are separated by sharp MGBs shown in green. The molecular director, following a nearly uniform rate of twist, produces a total twist Δ across each smectic block, with essentially no twist in the MGBs. (*b*) Contour plot of $F(\Delta, \alpha\beta = l_b k_o)$, the energy density of a GBTGBA relative to the SmA, as a function of l_b and Δ. $F(\Delta, \alpha\beta) > 0$ (colored black) and $\Delta(\alpha\beta)_{min}$, the local minimum of $F(\Delta, \beta)$ (colored yellow), follows a straight line corresponding to a mean twist equal to that preferred by the CN, i.e., with $\langle d\theta/dx\rangle = \Delta/l_b = k_o$. Energy cross sections are plotted for $\Delta = 2.0$ rad and $F_m(\Delta(\alpha\beta))$ along the minimum energy trough, showing the latter to be very shallow and broad (note the energy scale difference), enabling wide variation in l_b with little cost in energy.

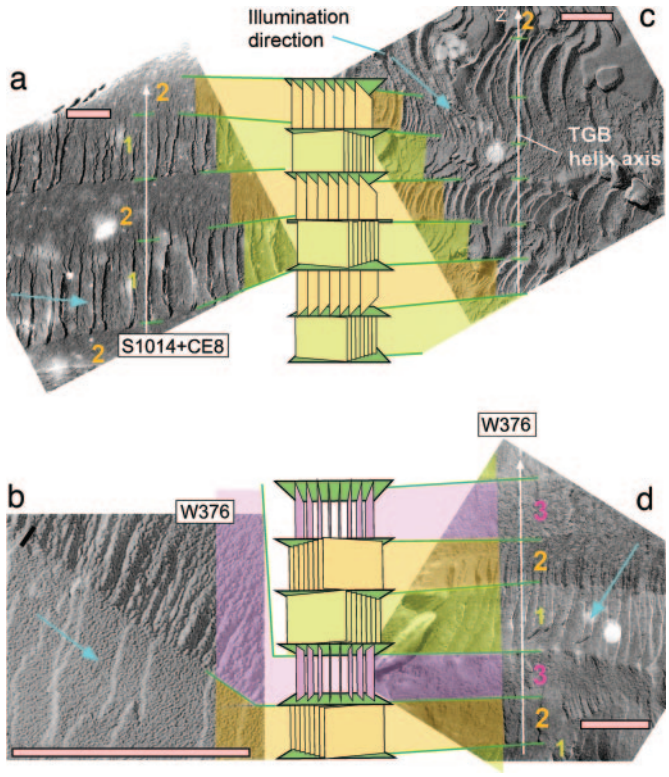

Fig. 2. FFEM images of S1014/CE8 and W376, with sketches of the corresponding GBTGB layer structures. Both materials exhibit regions of two-block ($\Delta = 90°$) or three-block ($\Delta = 60°$) periodicity, as shown for W376 in *c* and *d*. The white arrows in *a*, *c*, and *d* indicate the direction of the TGB helix, with the blue arrow showing the effective illumination direction for shadowing of the surface topography. MGBs are labeled with green lines. The scale of each image is indicated with a 400-nm-long pink bar. (*a*) $\Delta = 90°$ structure of S1014/CE8 freeze-fractured at 68°C in its TGBA phase ($p_{90} = 1{,}220$ nm at $T = 68°C$). (*b*) W376 fractured at 50°C in the TGBC phase showing the MGB, the 40-nm-long black line clearly significantly larger than the MGB width. (*c*) $\Delta = 90°$ structure of W376 in its TGBC phase ($p_{90} = 730$ nm at $T = 60°C$). (*d*) $\Delta = 60°$ structure of W376 in its TGBC phase ($p_{60} = 100$ nm at $T = 50°C$).

identifiable but distorted (Fig. 2*c*), as well as highly disordered regions. The FFEM study shows that these materials exhibit nearly identical patterns of block structure that are quite different from those found previously in TGBs, e.g., in the nP1M7 series (4), as follows: (*i*) In the GBTGBs the block size l_b is in the range $200\text{ nm} < l_b < 2{,}000$ nm, i.e., is very large, and is maximum in the disordered regions. (*ii*) The layers in the blocks are planar right up to the GBs, which are quite narrow, $\lesssim 5$ nm in width (Fig. 2*b*), much narrower than the blocks. The GBs show no evidence for screw dislocation structures, indicating that the screw dislocation spacing and accompanying modulation of layer structure is subresolution, and thus that the dislocation Burgers vector is small, most likely $b = 1$, or that there simply are no screw dislocations and the GB is nematic. (*iii*) The angular jumps in layer orientation between the blocks, Δ, are also large and can exhibit distinct types of commensurability, as evidenced by patterns of identical block orientation with 2-fold ($\Delta = 90°$, Fig. 2 *a* and *c*) and 3-fold ($\Delta = 60°$, Fig. 2*d*) periodic repeats in both GBTGB materials studied. With such large angular jumps between blocks and $b = 1$, the effective screw dislocation spacing l_d in the grain boundaries is comparable to or less than the layer spacing d ($l_d = d$ for $\Delta = 60°$), motivating the use of a GB model in which the dislocation cores strongly overlap, i.e., approaching a melted GB (MGB) description, that for which the average magnitude of the smectic order parameter is zero at the GB center (15). (*iv*) The layer normal **N** (Fig. 1) lies in the *y*-*z* plane normal to the TGB helix axis *x*. Thus the GBTGBC phases studied have the Renn/Lubensky-proposed TGBC layer structure, in contrast to previously studied TGBCs in which **N** makes an angle ω_L with respect to the *y*-*z* plane (16, 17).

The XRD experiments provide additional evidence for these key GBTGB structural features in W371 and W376. The scattering from W371 is especially interesting as it has a CN–GBTGBA–GBTGBC phase sequence, where the A-layer spacing, d_A, is nearly T-independent, and the C-layer spacing, d_C, exhibits a continuous contraction caused by molecular tilt, θ, of **n** from the local layer normal **N**, indicative of a second order GBTGBA–GBTGBC transition. This contraction can be determined from scans of $I(q_x, q_z)$ at $q_x = 0$, which show resolution-limited scattering peaks vs. $q_z = 2\pi/d$ (Fig. 3*a*), yielding an x-ray-determined tilt, $\theta_{x\text{-ray}} = \cos^{-1}(d_C/d_A)) = 21°$, at $T = 20°C$, a value that compares well with the optical tilt found in the electric field-induced smectic C (SmC) phase (6). In previous studies of the TGBA–TGBC-phase sequence, e.g., in the $nF_2BTFO_1M_7$ family (16), this layer contraction was found to be accompanied by layer tilt, evidenced by the evolution of the scattering from a single peak in q_x at $q_x = 0$, implying $\omega_L = 0$ in the TGBA, to a pair of peaks split in q_x in the TGBC. The fact that these split peaks are maximum along the line $q_z = 2\pi/d$ shows that $\omega_L = \theta_{x\text{-ray}}$, and thus that the layer tilt of **N** from the *y*-*z* plane is driven by the layer contraction (16). This layer tilting mechanism is identical to that driving formation of the chevron layer structure in the SmC phase in surface-stabilized ferroelectric LC cells (18, 19), where adhesion of the layers to the

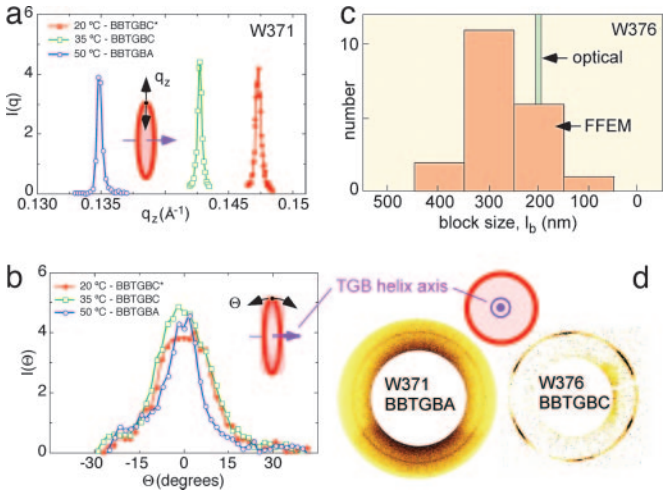

Fig. 3. Structural features of GBTGB phases. (*a* and *b*) XRD intensities from a Grandjean-oriented W371 sample. (*a*) The radial scans are resolution-limited and show the layer contraction through the GBTGBA–GBTGBC transition. (*b*) Despite this layer contraction, the layer normals remain perpendicular to the TGB helix axis. (*c*) Size distribution of block size l_b observed in well ordered TGB domains via freeze-fracture images of W376 at $T = 60$°C. FFEM gives somewhat larger l_b than that obtained from the optical measurement of the pitch because the fracture can be somewhat oblique to the TGB helix axis. (*d*) 2D detector images of the angular distribution of intensity about the TGB helix axis. The W371 sample is polydomain averaging to a ring even in the $\Delta = 90°$ GBTGB* phase at $T = 20$°C. The W376 sample is a monodomains exhibiting commensurate lock-in at $\Delta = 60°$.

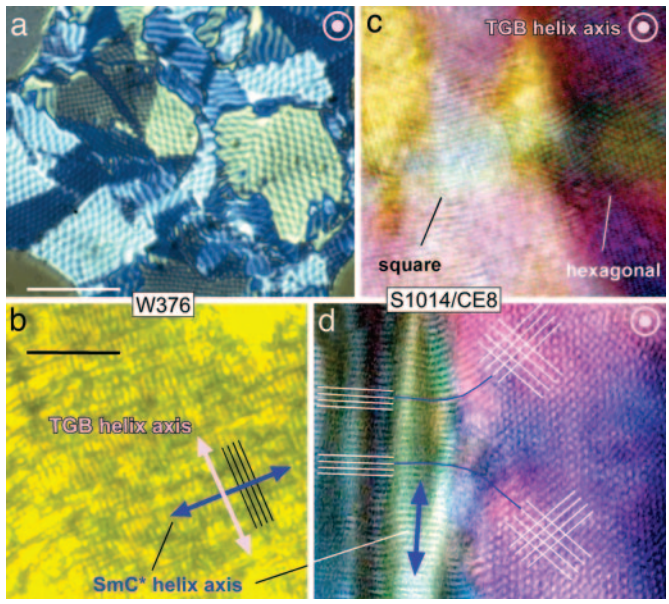

Fig. 4. Polarized light micrographs of the TGBC phase of GBTGB materials in transmission. The TGB helix axis is indicated in white and the SmC helix in blue. (*a*) Grandjean texture of a 2-μm-thick cell of W376 in the GBTGBC phase, showing areas of $\Delta = 60°$ and 90° periodicity. (*b*) Planar-aligned W376 with the TGB and SmC helices in the plane of the cell plates, showing orthogonal quasiperiodic arrays of lines from both helices. (*c*) Four-micrometer cell of S1014/CE8 clearly showing the SmC helix. The dark domain to the left contains a single smectic block (bookshelf alignment) that splits into two blocks on the right, rotated ≈60° from one another. This Δ is preferred, but only weakly, as *d* shows, with 60° domains merging into 90° domains over ≈100 μm. (Scale bars: 20 μm, *a* and *b*; 10 μm, *c* and *d*.)

surface plates requires maintenance of the smectic A (SmA)-layering wavevector component constant along z, which in turn requires tilt of the SmC layers when they are thin. Apparently, an equivalent adhesion mechanism is in force at the GBs in TGBC materials such as $11F_2BTFO_1M_7$ (16). However, W371 shows fundamentally different behavior, with $I(q_x, q_z)$ exhibiting resolution-limited scattering peaks vs. $|q|$ on arcs of constant $|q| = 2\pi/d$ as Θ, the angle between q and the y-z plane, is varied, with maximum peak intensity in $I(q, \Theta)$ at $\Theta = 0$ at all Ts in the A and C phases (Fig. 3*b*). This scattering structure indicates that diffraction broadening $\delta q_x \approx 1/l_b$ is negligible, a result of the large block size, and that $I(q_x, q_z)$ is the result of a mosaic probability distribution of smectic layer normals $P(\omega_L) \propto I(q, \Theta)$, where $P(\omega_L)$ is peaked at all T at $\omega_L = 0°$ and has a maximum half-width-at-half-height $\delta\omega_L \approx 10°$ at $T = 20$°C in the GBTGBC phase.

This difference may indicate that the GBs are melted in W371. Materials such as $11F_2BTFO_1M_7$ have low-angle ($\Delta \approx 0.1$) GBs across which layers are connected between dilute screw dislocations (20), spaced by l_d. For layers to shrink without tilting about y the screw dislocation spacing must correspondingly change ($l_d \propto l_b$), requiring nucleation of new dislocations and dislocation motion. By contrast, in the MGB case, the GB is a melted nematic-like film that isolates layers from those in adjacent blocks with respect to their translational displacement along **N**, effectively providing a lubricated interface.

The scattering from the W371 Grandjean samples was found to be independent of sample orientation about the TGB helix axis in the GBTGBA (Fig. 3*d*) and GBTGBC phases, even for $T < 35$°C, where the square grid modulation, indicative of $\Delta = 90°$ lock-in in the GBTGBC has appeared. This apparent isotropy was because the W371 modulation pattern was polydomain within the 1×1-mm illuminated area. However, it was possible to illuminate single modulation domains in W376, and these exhibited a 6-fold intensity modulation pattern indicative of $\Delta = 60°$ lock-in. Like W371, the scattering from W376 in the GBTGBC phase is also peaked at $\Theta \approx 0°$.

Fig. 3*c* shows a distribution of block sizes in W376 at $T = 60$°C, obtained from sampling $\Delta = 60°$ domains in the FFEM images, along with the l_b obtained from optical measurement of the TGB helix pitch p_{opt} of a $\Delta = 60°$ domain in a wedge-shaped Grandjean cell, and use of $l_b = p_{opt}\Delta/2\pi$ ($p_{opt} = 1{,}200$ nm). Tilt of the fracture plane with respect to the TGB axis tends to make the FFEM l_b values appear to be larger.

Depolarized transmission light microscopy observations in different cell geometries enable optical study of the TGB helix and smectic block structure under a variety of confinement conditions. In cells with the LC in a wedge-shaped gap between glass plates, Grandjean lines can be used to measure the TGB helix pitch, which increases with decreasing T in all of the materials studied (7). However, for thinner cells with the LC between rubbed nylon on indium tin oxide-coated glass plates, the behavior is quite different, as exemplified by the textures obtained with S1014/CE8 in a $t = 4$-μm thick gap (Fig. 4 *c* and *d*). In these cells the CN aligns in a Grandjean texture but, upon cooling, the appearance of smectic order at $T \approx 75$°C unwinds its helix nonuniformly, with the spontaneous formation of minority domains with no helix, i.e., with a single block (bookshelf alignment, $N_b = 1$) between the plates, and the majority of the cell with two blocks, $N_b = 2$, as shown in Fig. 4*d*. A $t = 4$-μm cell with the bulk pitch should have $N_b = \approx 14$ blocks. The layer orientation of the blocks formed near the CN–SmA is maintained upon cooling throughout the smectic T-range, remaining unchanged at the SmA–SmC transition where the SmC tilt of **n** develops and the SmC* helix (21) appears within the blocks, the * notation denoting the presence of the helix, the chiral precession of n around the tilt cone of angle θ (Fig. 1*a*). The SmC* helix not only renders the layer orientation visible (Fig. 4), but also, with electric field application to unwind the helix (22, 23), enables counting of the number of blocks, N_b. Thus, in the N_b = two domains two unwinding transitions are observed, generally with

PHYSICS

different threshold fields, indicating that the two blocks have different thickness since the field unwinding threshold depends on block thickness, decreasing with decreasing l_b (24). Block thickness is nonuniform, i.e., the position of the block–block interface between the plates varies across the cell, as is also the case for the two smectic blocks that appear in chiral SmA materials with a large surface electroclinic effect (25). In the two-block domains the layers of the two blocks are generally oriented symmetrically with respect to the rubbing direction (Fig. 3*d*), but this preference is weak, with local structures in some areas of the cell varying continuously to other regions with different angular jumps in orientation between the blocks ranging over $0 < \Delta < 90°$ (Fig. 4*c*). Areas with either $\Delta = 60°$ or $\Delta = 90°$ are also observed, in agreement with the FFEM observations. In $N_b =$ two domains the TGB helix is maintained in a partially unwound condition by the influence of the rubbed polymer surfaces on the director. The possibility of accommodating such reduced twist along the TGB helix axis in the SmA by introduction of a single high-Δ GB provides direct evidence that λ is large ($\lambda k_o \approx 1$), as will be discussed below. The W376 2D lattice structures (Fig. 4*a*) are similar to that found in planar preparations of S1014/CE8 (ref. 7 and Fig. 4*d*). W376 and W371 also showed Grandjean textures similar to those of S1014/CE8 in $t <$ 5-μm cells. For example, Fig. 4*a* shows a $t \approx$ 2-μm-thick W376 Grandjean cell (planar smectic alignment on the surfaces) with distinct areas of different block number exhibiting square and nearly hexagonal lattices.

It was also possible to obtain cells of W376 between plates coated for homeotropic orientation of the director that gave the TGB helix parallel to the glass. This optical texture, smooth focal conic arrays in the CN phase as expected for a short-pitch CN, enabled the local CN helix axis to be determined unambiguously. These cells develop distinct quasiperiodic bands running normal to the CN helix upon cooling into the TGBA phase, which we interpret as the appearance of blocks to form a TGB helix (Fig. 4*b*). Upon further cooling in the TGBC phase a second set of stripes, the SmC* helix, appears normal to the first (Fig. 4*b*). This texture shows regions of distinct correlation in SmC* helix position through a distance of many TGB blocks along the TGB helix axis, suggestive of lock-in to a commensurate structure of the TGB block orientation. The resulting texture (Fig. 4*b*), however, is quite spatially inhomogeneous, which we ascribe to the spatial variation of Δ and l_b, and perhaps lock-in with different Δ values in different places.

Discussion

Development of a model for GBTGBA behavior begins by noting that the CN elastic energy is lowered as the nematic-preferred twist wavevector k_o is approached everywhere, and the smectic energy is minimized by reducing the number of grain boundaries, i.e., increasing l_b. These conditions tend to maintain $\lambda \approx l_b$, to avoid untwisted domains in the block centers, which typically suppress the TGB phase altogether if the GB energy cost forces $l_b > \lambda$. With the freeze fracture data showing $\Delta = k_o l_b \approx 1$, so that $l_b \approx 1/k_o$, we then expect that $\lambda \approx l_b \approx 1/k_o$ is the basic condition characterizing the GBTGBs, which, given that the layers in the blocks are planar and the GBs (typically of dimension ξ) are sharp, implies that $\lambda, l_b \gg \xi$. In such a structure, the twist of **n** must occur essentially entirely within the blocks, as sketched in Fig. 1*a* for the GBTGBA phase. Also, as noted above, for the large Δs observed the dislocation spacing in the GBs is $<d$, motivating a MGB description of the GBs (15), which accounts for the suppression of smectic ordering the GB but ignores its internal periodicity.

The large separation of length scales between block and GB thickness and negligible director twist within the GBs enables independent theoretical treatment of the block twist and GB structures. The simplest approach to calculating the GB energy/area, E_{GB}, is from the Landau-deGennes energy of smectic ordering (21): $2F_s = a[-|\psi_o|^2 + |\psi_o|^4/2\psi_o^2 + (\xi^2)(\partial\psi_o/\partial x)^2 + (\xi^2)(q_o\theta)^2]$, where ψ_o is the bulk value of the smectic order parameter magnitude, $|\psi|$, ξ is the transverse correlation length for smectic ordering, $q_o = 2\pi/d$, and $a(T)$ is the energy scale for smectic layering. The structure of an MGB is obtained by setting $\theta = 0$ in F_s, and solving the Euler equation with the boundary conditions $|\psi| = 0$ at $x = 0$ and $|\psi| = \psi_o$ at $x = \infty$. The resulting GB is of thickness $\approx 2\xi$, with $E_{GB} = 2a\psi_o^2\xi$ (26), sketched in Fig. 1*a*.

The TGBA twist structure within the blocks, given by $\theta(x)$, the tilt of the director **n** from the layer normal **N**, can be calculated from the energy density $F_n(\theta,\partial\theta/\partial x) = (K/2)[(\partial\theta/\partial x)^2 - 2k_o\partial\theta/\partial x + \theta^2/\lambda^2]$, where k_o is the nematic-preferred wavevector for twist of n ($P = 2\pi/k_o$ in the absence of smectic ordering), K is the nematic twist elastic constant, and the third term is the transverse part of F_s, in which $K/\lambda^2 = a\psi_o^2(\xi q_o)^2$ is the susceptibility for tilt of **n** from **N**. For $\lambda \to \infty$, $F_n = F_I = -Kk_o^2/2$, the nematic energy of the ideal helix relative to the unwound smectic state. Assuming an isolated chiral SmA block in the absence of external surface torques on **n** gives $\theta(x) = (\Delta/2)\sinh[(\beta/2 - x/\lambda)]/\sinh(\beta/2)$, where $\beta = l_b/\lambda$, $x = 0$ is taken to be at the block edge, as sketched in Fig. 1*a*, and $F_n(\Delta, l_b, \lambda)$ is minimized for $\Delta_{\min}(k_o, l_b, \lambda) = 2\alpha\tanh(\beta/2)$, with $\alpha = \lambda k_o$. In this model the MGBs transmit no torque on the director, the director field within the blocks depending only on l_b once k_o and λ are specified.

The structure of the single GB in the $N_b =$ two domains of Fig. 4 *c* and *d* can now be obtained by letting $l_b \to \infty$ in the above expression and noting that, in the block at the remaining single GB near $x = 0$ (Fig. 1*a*), the net director twist is $\Delta/2 = \alpha = \lambda k_o$. Thus, in this case the preferred net twist across the single $N_b =$ two-domain GB, i.e., including the boundaries of its two blocks, will be $2\lambda k_o$. Experimentally then, $\pi/3 < 2\lambda k_o < \pi/2$, requiring $\lambda k_o \approx 0.5$. Since in the TGB structure with nearly the preferred CN pitch (e.g., the TGBA of S1014/CE8) we must necessarily have $k_o = \Delta/l_b$, we immediately find that $\lambda \approx l_b/2$ for the observed GBTGB values of $\Delta \approx 1$. Thus, in the GBTGBs studied here the twist penetration length is comparable to the giant block size.

The energy density of a bulk TGB phase, a periodic array of such twisted smectic blocks, is the sum of the nematic elastic and GB contributions:

$$F(\Delta, \beta, \alpha)/Kk_o^2 = (1/2)[\tanh(\beta/2)/(\beta/2)][(\Delta/\Delta_{\min})^2 - 2\Delta/\Delta_{\min}] + 2\varepsilon(\xi/\lambda)(1/\beta), \quad [1]$$

where $\varepsilon = a\psi_o^2/Kk_o^2$ is the ratio of smectic-to-nematic energy scales. $F(\Delta, \beta, \alpha)/Kk_o^2$, plotted in Fig. 1*b* vs. Δ and $\alpha\beta = l_b k_o$ for several values of α, $\psi_o = 0.5$, $K = 3 \times 10^{-8}$ J/m, and $\varepsilon = 0.06$; although too simple to be considered as anything more than an elementary TGB description, nonetheless it illustrates several important features of TGB energetics relevant to the GBTGBs. Specifically, for the range of Δ of interest ($0.15 < \Delta < 1.5$ rad), $F(\Delta, \beta, \alpha)$ exhibits a minimum $F_m(\Delta(\alpha\beta))$ along the line $l_b k_o = \Delta$ (see the blue line in Fig. 1*b*), corresponding to the preferred CN twist. $F_m(\Delta(\alpha\beta))$ increases at small Δ because of the increasing number of GBs, and at large Δ because of increased deviation of **n** from the ideal linear helix (see red curves in Fig. 1*b*). While the minimum in $F(\Delta, \beta, \alpha)$ vs. l_b is deep (see the black curve in Fig. 1*b* along $\Delta = 2$ rad), the minimum in F_m along the line of preferred twist is comparatively quite weak (note the reduced energy scale at left for the red curves in Fig. 1*b*), especially for $\lambda \approx 1/k_o$ and $l_b \lesssim \lambda$, in which case there is little energetic penalty to pay for increasing l_b along the line of preferred twist to $l_b \approx \lambda$. For larger l_b, untwisted regions appear in the middle of the blocks at $|x| > \lambda$ from the GBs and the energy increases rapidly. This energy analysis and the observation of thick blocks in the $N_b =$ two domains of S1014/CE8 suggest that the GBTGB structure has l_b comparable to a few λ. The assumption that the GBs are melted and thus that GB energy is independent of Δ is likely to be met only for large angle GBs ($\Delta \approx 1$). For small Δ the screw dislocation interactions must be accounted for (1, 27).

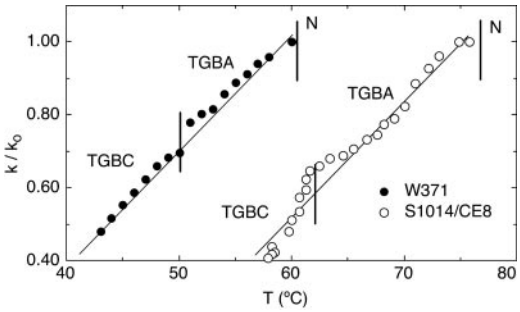

Fig. 5. Temperature dependence of k/k_o, the GBTGB helix wavevector k divided by its value k_o at the CN/GBTGB transition in S1014/CE8 and W371. k/k_o is approximately linear vs. T with similar slopes in the two materials, with deviation from linearity associated with the appearance of the intrablock SmC helix in the GBTGBC phase. Linear behavior indicates that $\eta \approx \delta G\xi/Kk_o$ and thus δG varies as $\delta G \approx T_{N/TGBA} - T$.

In the GBTGBC case, where local energy is minimized with **n** tilted from **N** through some equilibrium angle θ_C, i.e., lying on the tilt cone of angle θ_C, the transblock twist is enabled both by azimuthal reorientation, $\varphi(x)$, of **n** into a polarization splayed/director twisted state (9, 28), as well as by spatial variation **n** away from the equilibrium orientation, as in the GBTGBA when λ is large. Detailed calculation of the twisted state with fixed θ_C (λ = 0), corresponding to free surfaces on a block (29) [in this reference ($\gamma_1 = \gamma_2 = 0$) with intrinsic twist $q_b \neq 0$] shows that the twisted state is always the most stable (ref. 29 and Fig. 5). Thus, for the GBTGBCs studied here ($l_b k_o = \Delta \approx 1$ and $\theta_C \approx \Delta$) the change in $\varphi(x)$ across a block is π, as described by Brunet *et al.* (9) [$\partial\varphi(x)/\partial x \approx \pi/l_b$], and the energetics of the elasticity are not significantly different from the GBTGBA detailed above in that the energy gained from twisting is still $\approx -Kk_o^2/2$. Similar gain is obtained for λ large so that in either case the GBTGBC energy dependence on $l_b k_o$ and Δ will be qualitatively similar to that of Fig. 1*a*.

Another GBTGB feature requiring theoretical discussion is the presence of the SmC* helix, generally observed to be expelled in TGBC phases with small blocks (16). However, the GBTGB case, with λ and l_b large, has not been considered in previous discussions of SmC*-helixed TGBs (9, 30–32). The structure and energetics of the helix within bounded smectic slabs has been considered since the earliest days of the study of chiral smectics, leading to quantitative criteria for its stability and confinement-induced unwinding, for example in surface-stabilized ferroelectric LC cells (24, 29 33, 34). In the present case, the general analysis of Brunet and Martinot-Lagarde (24) can be applied to the case of smectic blocks with $\lambda \approx l_b$. We pursue an approximate description, considering perturbations of the basic GBTGBA structure of Fig. 1*a*, which appear upon entering the GBTGBC. For a TGBC block with director tilt θ_C and azimuthal orientation φ, the energy density of the SmC* helix for the case of free boundaries is $F_h \approx (K\theta_C^2/2)[(\partial\varphi/\partial z)^2 - 2k_C(\partial\varphi/\partial z)]$, where $k_C = 2\pi/p_C$ is the wavevector of the SmC* helix. The condition for helix unwinding in the block is obtained by comparing the resulting energy minimum of the wound helix, $F_{hmin} \approx -(K\theta^2/2)k_c^2$ with the cost of satisfying boundary conditions caused by the finite block size, assuming a SmC tilt susceptibility comparable to that of the SmA, i.e., $\lambda_C \approx \lambda$. For a SmC slab of thickness d_C with φ fixed at the grain boundaries (i.e., the director tilt lies in the plane of the GBs) as in Fig. 1*a*, we obtain the approximate unwinding thickness $d_C \approx \sqrt{\lambda_c \rho_c}$. This is the result of comparing the energy gain of winding the helix with the energy cost of the cores (of dimension λ) and the bulk distortion in λ of the resulting required line disclinations, leading to the condition expressed on page 1707 of ref. 24. However, in the GBTGB case φ at the block boundaries is not fixed, but determined by a finite anchoring energy of strength $U \approx K/\lambda_C$, i.e., with a surface interaction length (26) also given by λ_C. Since the helical winding of the director in a given block provides little energy relief in its neighbors (since their difference in layer normal orientation is $\Delta > 60°$), the deformation caused by this block relaxes away in a distance λ away from the block, effectively making each block thicker by λ_C at each of its two interfaces with a GB. In this picture, each block has its own SmC helix, with "tails" decaying over a distance roughly λ_C into its neighboring blocks. If $\lambda_C \approx l_b/2$, then the effective Brunet and Martinot-Lagarde slab thickness is $d_c \approx 4\lambda_C$ and the SmC* helix will be present as long as $p_C \lesssim 16\lambda$. For the l_bs of the materials studied this gives p_C up to $p_C \approx 2\ \mu$m, comparable to that found in W376 (Fig. 4) and S1014/CE8 (7). The nematic orientation in each GB is modulated to be commensurate with the helices in both adjacent blocks. As discussed by Pramod *et al.* (35), this is a likely mechanism for the observed transverse periodic undulation in the x-position of the GBs (7). In this case, the dark/light stripes shown in figure 4*d* of ref. 7 are caused by a $\Delta = 90°$ structure of blocks alternating between having **N** parallel to and normal to the image plane. The coupling of $\varphi(r)$ between neighboring blocks also provides a possible mechanism for the preference of $\Delta = 60°$ or 90° orientational jumps, either by coupling of fluctuations in GBs or SmC* helix penetration. Given the energetic ambivalence with respect to the choice of Δ and l_b, indicated by Fig. 1*b*, even weak second-nearest neighbor interactions could stabilize commensurate lock-ins.

The large penetration length ($\lambda \approx 100$ nm) deduced from our experiments shows that a key GBTGB material parameter is a large susceptibility for tilt of **n** from the layer normal even in the SmA phase near the SmA–CN phase transition. This finding implies a large, weakly temperature-dependent electroclinic coefficient $e = \partial\theta/\partial E$ for field-induced tilt, which has been observed in SmA W371, ranging from $e = 0.8°/(\mathrm{V}/\mu\mathrm{m})$ at the SmA–CN transition to $1.5°/(\mathrm{V}/\mu\mathrm{m})$ at the SmA–SmC transition (6), comparable to the largest values of e ever observed over wide T ranges (36–38), and $e \approx 0.2/(\mathrm{V}/\mu\mathrm{m})$ in S1014/CE8 (39). These observations were made in the SmA state after unwinding the TGBA helix with an electric field (6). The fact that the helix can be unwound by applied field, also observed in W376, is itself a feature of large electroclinic response. A universal aspect of such large-e electroclinic materials is saturation of $\theta(E)$ at large E (38–40), typically at $\theta \approx 30°$, indicating that $(\partial\psi/\partial x)^2$ or other higher-order terms that act to limit θ need to be added to the harmonic Landau–deGennes expression for $\psi(x)$ above. Such terms will similarly act to limit Δ and would also influence the spatial gradients of $|\psi(x)|$ and thus the effective correlation length ξ. In the harmonic Landau–deGennes approximation, since $\lambda \approx \xi^{-1}$, large λ implies small x. For the λ values observed ($\lambda k_o \approx 1$), we find the ratio of smectic-to-nematic energy scales $\varepsilon \approx 1$, therefore $q_o\xi \approx 1$, implying that $\xi < d$, the layer spacing. The addition of higher order $\partial\psi/\partial x$ terms would bring ξ into a more physically reasonable range ($\xi \approx d$).

The large linear electroclinic susceptibility at low $\theta(E)$ and nonlinear saturation at large $\theta(E)$ suggests an even simpler extreme nonlinear "square well (SW)" model of the GBTGB structure, wherein the energy cost of tilt within a block is assumed to be zero (infinite tilt susceptibility) for $\theta(E)$ in the range $-\theta_{sat} < \theta(E) < \theta_{sat}$ and to be infinite for $|\theta(E)| > \theta_{sat}$, where θ_{sat} is a property of the smectic layering. We assume again that the blocks are bounded by MGBs that transmit no torque on the director, so that the reorientation across each block is always from $-\theta_{sat}$ to $+\theta_{sat}$. Within the blocks this model yields simple twist of the director of wavevector $k = (\partial\theta/\partial x) = (2\theta_{sat}/l_b)$, and an angle jump $\Delta = 2\theta_{sat}$ at the MGBs. Assuming MGBs of energy $F_{MGB}(l_b) = \delta G\xi/l_b$, where δG is the CN–SmA free energy difference and ξ the CN–SmA interface thickness, the free energy $F_{SW}(l_b)$ results

$$F_{SW}(l_b) = (K/2)[2\theta_{sat}/l_b) - k_o]^2 + \delta G\,\xi/l_b \qquad [2]$$

$$F_{SW}(y)/Kk_o^2 = (1/2)[(1/y) - 1]^2 + \eta/y, \qquad [3]$$

where $y = k_o l_b/2q_{sat}$ and $\eta = \delta G\xi/(2\theta_{sat}Kk_o)$. This leads to a TGB state with pitch

$$k(T)/k_o = 1 - \eta(T) \quad [4]$$

for $\eta < 1$, the unwound SmA state for $\eta > 1$, and $y = 1$ ($l_b = 2\theta_{sat}/k_o$) the block size in the limit of small δG. In this model, taking $2\theta_{sat} \approx 1$, the basic condition for obtaining the GBTGB is $\delta G\xi < Kk_o$, the GB energy cost/area needs to be less than the helix twist energy gain/area. Eq. **2** yields qualitatively similar dependence of F on $k_o l_b$ as the large λ model above. Helix pitch data on S1014/CE8 (7) and W371, plotted in Fig. 5, show that $\eta(T) \propto T_{N/TGBA} - T$, which is to be expected if the dominant T dependence of η is that of $\delta G \approx T_{N/TGBA} - T$, where $T_{N/TGBA}$ is the CN/TGBA transition temperature. S1014/CE8 and W371 exhibit similar dependence on T, indicating that $\eta(T)$ grows to ≈0.5 at $T_{NA} - T = 20$°C in both materials.

A further consequence of the significant twist within the blocks appearing as a result of the large tilt susceptibility in the GBTGBA is a substantial tilt $\theta(x) \approx 30°$ of **n** away from **N** at the edges of the blocks (Fig. 1*a*), but no tilt ($\theta \approx 0$) in the middle of the blocks (Fig. 1*a*). One might then expect to find a variation in the layer thickness $d(x) \approx d\cos[\theta(x)]$ across the block, especially in W371, which exhibits significant layer contraction at the A–C transition. However, no such variation is seen, as the peaks in the radial wavevector x-ray scans through the TGB ring remain resolution-limited in the W371 and S1014/CE8, even though exhibiting significant shift in position upon passing from the SmA to the SmC phase, e.g., as in the W371 data in Fig. 3*a*. This may be an indication of "deVries"-type SmA behavior (37, 40), the azimuthal orientational ordering about the layer normal of already tilted molecules (requiring an explanation of the contraction found in the C phases), or it may reflect the energy cost of introducing edge dislocations into the blocks (requiring an explanation for why the tilt susceptibility is still so large at constant layer spacing).

Another interesting characteristic of the GBTGBs is their large TGB temperature ranges (10°C < T_R < 100°C). In the small block systems, the TGB phase gives way to a uniform untwisted smectic on cooling, a consequence of increasing energy cost of the GBs ($E_{GB} \propto \sqrt{a}$ in the Landau–deGennes harmonic model), resulting in larger l_bs as the smectic order strengthens. As l_b increases beyond λ, the increasing deviation of the twist from an ideal helix raises the overall energy above that of the untwisted smectic. However, the effect of increasing λ (for example, by decreasing ξ at constant $a|\psi_o|^2$) is always to reduce the distortion in the twist of **n**, making accommodation of the twist in the smectic easier by moving the nematic energy closer to the $F_I = -Kk_o^2/2$ of the ideal helix, behavior evident in the model calculation of Fig. 1*b*. Additionally the number of GBs required is reduced. These factors combine to make large λ TGB states more energetically favorable for a given k_o, rendering the TGB stable even with a saturated smectic order parameter.

Conclusion

To conclude, experiments on several examples of the subclass of chiral smectic LC materials exhibiting wide TGB phase ranges and TGBC phases with the SmC helix have enabled us to provide basic information on the origin of this behavior. We show that the key relevant properties of such materials are a large tilt susceptibility λ^2/K and a large penetration length λ for tilt of the director, the latter being comparable to k_o^{-1}, the inverse wavevector of the CN twist. This, in turn, leads to the bulk condition that the smectic blocks are giant, with thickness l_b also comparable to λ and k_o.

The GBs observed here are sharp and planar, mediating large angle jumps between flat layers, indicating that if the screw dislocations exist they are well ordered into periodic arrays [rather than strongly fluctuating (41)]. The data and analysis, however, do not produce a detailed understanding of the internal structure of the GBs, i.e., whether the average smectic order parameter becomes small enough in the GB centers to consider them melted, and to what extent there is electron density modulaton within the GBs because of screw dislocations. The types of few block cells presented in Fig. 4*c* may offer an opportunity to address the latter question with microbeam XRD experiments on single GBs. The model, based on MGBs, describes the general GBTGB phenomenology well, but answers to remaining questions, such as the origin of the $\Delta = 60°$ and 90° lock-in, will require a more complete theoretical description of the large λ limit.

We thank T. Sluckin and T. Lubensky for conversations. This work was supported by National Science Foundation Grants DMR 0072989 and DMR 0213918 (Materials Research Science and Engineering Centers).

1. Renn, S. R. & Lubensky, T. C. (1988) *Phys. Rev. A* **38,** 2132–2146.
2. Goodby, J., Waugh, M., Stein, S., Chin, E., Pindak, R. & Patel, J. (1989) *Nature* **337,** 449–452.
3. deGennes, P. G. (1973) *Solid State Commun.* **8,** 753–756.
4. Ihn, K. J., Zasadzinski, J. A., Pindak, R., Slaney, A. J. & Goodby, J. (1992) *Science* **258,** 275–278.
5. Navailles, L., Barois, P. & Nguyen, H. T. (1993) *Phys. Rev. Lett.* **71,** 545–548.
6. Shao, R., Pang, J., Clark, N., Rego, J. & Walba, D. (1993) *Ferroelectrics* **147,** 255–262.
7. Pramod, P. A., Pratibha, R. & Madhusudana, N. V. (1997) *Curr. Sci.* **73,** 761–765.
8. Ribeiro, A., Barois, P., Galerne, Y., Oswald, L. & Guillon, D. (1999) *Eur. Phys. J.* **11,** 121–126.
9. Brunet, M., Navailles, L. & Clark, N. (2002) *Eur. Phys. J.* **7,** 5–11.
10. Dierking, I. (2001) *Liq. Cryst.* **28,** 165–170.
11. Kuczynski, W. & Stegemeyer, H. (1995) *Mol. Cryst. Liq. Cryst.* **260,** 377–386.
12. Kitzerow, H. S., Slaney, A. J. & Goodby, J. W. (1996) *Ferroelectrics* **179,** 61–80.
13. Gulik-Krzywicki, T. & Costello, M. J. (1978) *J. Microsc.* **112,** 103–113.
14. Zasadzinski, J. A. (1990) *J. Phys.* **51,** 747–756.
15. Dozov, I. (1995) *Phys. Rev. Lett.* **74,** 4245–4248.
16. Navailles, L., Pindak, R., Barois, P. & Nguyen, H. T. (1995) *Phys. Rev. Lett.* **74,** 5224–5228.
17. Bouchta, A., Nguyen, H. T., Navailles, L., Barois, P., Destrade, C., Bougrioua, F. & Isaert, N. (1995) *J. Mat. Chem.* **5,** 2079–2092.
18. Rieker, T. P., Clark, N. A., Smith, G. S., Parmar, D. S., Sirota, E. B. & Safinya, C. R. (1987) *Phys. Rev. Lett.* **59,** 2658–2661.
19. Rieker, T. P. & Clark, N. A. (1992) in *Phase Transitions in Liquid Crystals*, ed. Martellucci, S. (Plenum, New York), pp. 287–342.
20. Kamien, R. D. (2002) *Rev. Mod. Phys.* **74,** 953–971.
21. deGennes, P. G. & Prost, J. (1993) *Physics of Liquid Crystals* (Clarendon, Oxford).
22. Glogarova, M., Fousek, J., Lejcek, L. & Pavel, J. (1984) *Ferroelectrics* **58,** 161–178.
23. Lagerwall, S. T. (1999) *Ferroelectric and Antiferroelectric Liquid Crystals* (Wiley, Weinheim, Germany), pp. 172–180.
24. Brunet, M. & Martinot-LaGarde, P. (1996) *J. Phys. II* **6,** 1687–1725.
25. Shao, R. F., Maclennan, J. E. & Clark, N. A. (2001) *Liq. Cryst.* **28,** 117–123.
26. Vaupotic, N., Copic, V. & Sluckin, T. J. (1998) *Phys. Rev. E* **57,** 5651–5659.
27. Bluestein, I., Kamien, R. D. & Lubensky, T. C. (2001) *Phys. Rev. E* **63,** 061702.
28. Handschy, M. A., Clark, N. A. & Lagerwall, S. T. (1983) *Phys. Rev. Lett.* **51,** 471–474.
29. Handschy, M. A. & Clark, N. A. (1984) *Ferroelectrics* **59,** 69–116.
30. Renn, S. R. & Lubensky, T. C. (1991) *Mol. Cryst. Liq. Cryst.* **209,** 349–355.
31. Renn, S. R. (1992) *Phys. Rev. A* **45,** 953–973.
32. Galerne, Y. (2000) *Eur. Phys. J.* **3,** 355–368.
33. Clark, N. A. & Lagerwall, S. T. (1980) *Appl. Phys. Lett.* **36,** 899–901.
34. Brunet, M. & Williams, C. (1978) *Ann. Phys. (Paris)* **3,** 237–248.
35. Pramod, P. A., Hatwalne, Y. & Madhusudana, N. V. (2001) *Liq. Cryst.* **28,** 525–533.
36. Spector, M. S., Heiney, P. A., Naciri, J., Weslowski, B. T., Holt, D. B. & Shashidhar, R. (2000) *Phys. Rev. E* **61,** 1579–1584.
37. Clark, N. A., Bellini, T., Shao, R. F., Coleman, D., Bardon, S., Link, D. R., Maclennan, J. E., Chen, X. H., Wand, M. D., Walba, D. M., *et al.* (2002) *Appl. Phys. Lett.* **80,** 4097–4099.
38. Williams, P. A., Komitov, L., Rappaport, A. G., Thomas, B. N., Clark, N. A., Walba, D. M. & Day, G. W. (1993) *Liq. Cryst.* **14,** 1095–1105.
39. Dhara, S., Pratibha, R. & Madhusudana, N. V. (2002) *Ferroelectrics* **277,** 13–23.
40. de Vries, A. (1977) *Mol. Cryst. Liq. Cryst.* **41,** 27–31.
41. Lubensky, T. C., Tokihiro, T. & Renn, S. R. (1991) *Phys. Rev. A* **43,** 5449–5462.